EPJ.org

○ EPJ Quantum Technology
a SpringerOpen Journal

Open Access

CrossMark

Hybrid optimization schemes for quantum control

Michael H Goerz[1], K Birgitta Whaley[2] and Christiane P Koch[1*]

*Correspondence:
christiane.koch@uni-kassel.de
[1] Theoretische Physik, Universität
Kassel, Heinrich-Plett-Str. 40, Kassel,
D-34132, Germany
Full list of author information is
available at the end of the article

Abstract

Optimal control theory is a powerful tool for solving control problems in quantum mechanics, ranging from the control of chemical reactions to the implementation of gates in a quantum computer. Gradient-based optimization methods are able to find high fidelity controls, but require considerable numerical effort and often yield highly complex solutions. We propose here to employ a two-stage optimization scheme to significantly speed up convergence and achieve simpler controls. The control is initially parametrized using only a few free parameters, such that optimization in this pruned search space can be performed with a simplex method. The result, considered now simply as an arbitrary function on a time grid, is the starting point for further optimization with a gradient-based method that can quickly converge to high fidelities. We illustrate the success of this hybrid technique by optimizing a geometric phase gate for two superconducting transmon qubits coupled with a shared transmission line resonator, showing that a combination of Nelder-Mead simplex and Krotov's method yields considerably better results than either one of the two methods alone.

Keywords: quantum control; optimization methods; quantum information

1 Introduction

Coherent quantum control has long been a key component in the effort towards future quantum technologies. It relies on the interference between multiple pathways to steer the quantum system in some desired way [1, 2]. Originally conceived for the control of chemical reactions [3–5], it has since been extended to a wide variety of applications, see Ref. [6] for a review. In this context, numerical optimal control theory (OCT) is a particularly powerful tool. OCT follows an iterative approach, improving the control field in each iteration to steer the dynamics to the optimization target. Generally, the fastest converging algorithms are those that take into account information about the gradient of the optimization functional with respect to variations in the control. Gradient-based methods assume an open-loop setup, where the entire optimization procedure is performed based on the knowledge of the system dynamics. Two widely used methods are Krotov's method [7–9] and gradient ascent pulse engineering (GRAPE) [10]. Krotov's method guarantees monotonic convergence for time-continuous control fields. The Limited memory Broyden-Fletcher-Goldfarb-Shannon (LBFGS) method [11] can be used to extend both GRAPE [12] and Krotov's method [13], considering not only the gradient but also an estimate for the Hessian, i.e., the second order derivative. This has been demonstrated to

improve the convergence in some instances, in particular when close to the optimum [14]. In experimental setups that only allow for limited control and knowledge of the dynamics, closed-loop control schemes have often been preferred [15]. There, the controls are updated based only on a measurement of the figure of merit, e.g. using genetic algorithms [16] or other gradient-free optimization methods.

More recently, gradient-free optimization methods have also been employed in an open-loop context, prompted by the observation that evaluation of the gradient in many-body systems is often numerically infeasible. The chopped random basis (CRAB) method [17, 18] has been formulated for such applications. It expands the control in a relatively small number of randomly chosen spectral components and then applies a Nelder-Mead simplex optimization to the expansion coefficients. In principle, gradient-free methods are applicable if the control can reasonably be described by only a few free parameters and the optimization landscape has no local minima in the vicinity of the initial 'guess'.

Optimal control theory is particularly relevant for quantum information processing. Both Krotov's method and GRAPE have been extensively used to obtain high-fidelity quantum gates [19–24]. Short gate durations are crucial, in order to minimize detrimental effects of decoherence. With OCT, this is achieved by systematically decreasing the gate duration until no solution can be found [25, 26], thus operating at the quantum speed limit [27, 28]. Moreover, OCT may be used to actively minimize the effects of decoherence [29, 30], and to increase robustness with respect to classical noise [31]. Robustness is a requirement that is generally difficult to fulfill with analytical approaches.

Here, we explore the possibility of combining gradient-free and gradient-based methods at different stages in the optimization, exploiting the benefits of each method. The application of a simplex optimization to a guess pulse, described by only a few free parameters, efficiently yields a comparably simple first optimized pulse of moderate fidelity. This pre-optimized pulse then provides a good starting point for further optimization using a gradient-based method. The second optimization stage relaxes the restrictions on the search space implied by a simple parametrization and may then quickly converge towards a high fidelity. The simplex pre-optimization addresses the observation that typically in direct gradient-based optimizations, due to the large size of the search space, the majority of the numerical effort is spent in 'getting off the ground'. Pre-optimization thus allows to locate a region of the search space in which the gradient is large enough to provide meaningful information. Such good guess pulses may sometimes be designed by hand, but this requires a very good intuition of the underlying control mechanisms. We propose here instead to simply prune the search space for the initial phase of the optimization by reducing the complexity of the control. The second optimization stage can then more easily identify high fidelity solutions.

We illustrate the use of such hybrid optimization schemes by optimizing a quantum gate on superconducting qubits, using an example inspired by the recently proposed resonator-induced phase gate [32]. Superconducting circuits are a prime candidate for the implementation of quantum computing, due to the flexibility in qubit parameters, their inherent controllability, and the promise of scalability. Moreover, with recent advances in the transmon architecture, decoherence times are approaching 0.1 ms [33], allowing to reach fault-tolerance with sufficiently fast gates. However, the flexibility and large number of different gate mechanisms [34] also imply a challenge from a control perspective, as it is not immediately obvious what are good qubit parameters, or good guess pulses. This makes

superconducting circuits especially well-suited for combining a coarse search using simplex methods, which may then be refined with a more powerful gradient-based method.

The paper is organized as follows: In Section 2, we review the realization of a geometric phase gate on a system of two transmon qubits coupled with a shared transmission line resonator, using all microwave control. In Section 3, we first introduce a functional targeting the geometric phase gate, i.e., any diagonal perfect entangler, and then show the results of a direct optimization using the gradient-based Krotov method. In Section 4, we apply the gradient-free Nelder-Mead simplex optimization to obtain pre-optimized guess pulses, which then become the starting point for an optimization with Krotov's method. We compare the control pulses obtained by the gradient-based, gradient-free, and hybrid schemes, and the dynamics they induce, as well as the numerical effort necessary to obtain converged results in each scheme. Section 5 concludes.

2 Model and gate mechanism

We consider a system of two transmon qubits, coupled via a shared transmission line resonator ('cavity') [35, 36]. The Hamiltonian reads

$$\hat{\mathbf{H}} = \sum_{q=1,2} \left[\omega_q \hat{\mathbf{b}}_q^\dagger \hat{\mathbf{b}}_q + \frac{\alpha_q}{2} \hat{\mathbf{b}}_q^\dagger \hat{\mathbf{b}}_q^\dagger \hat{\mathbf{b}}_q \hat{\mathbf{b}}_q + g_q \left(\hat{\mathbf{b}}_q^\dagger \hat{\mathbf{a}} + \hat{\mathbf{b}}_q \hat{\mathbf{a}}^\dagger \right) \right] + \omega_c \hat{\mathbf{a}}^\dagger \hat{\mathbf{a}} + \epsilon^*(t)\hat{\mathbf{a}} + \epsilon(t)\hat{\mathbf{a}}^\dagger, \qquad (1)$$

where $\omega_c, \omega_1, \omega_2$ are the frequency of the cavity and the first and second qubit, respectively; α_1, α_2 are the qubit anharmonicities, and g_1, g_2 are the coupling between each qubit and the cavity. The operators $\hat{\mathbf{a}}$, $\hat{\mathbf{b}}_1$, and $\hat{\mathbf{b}}_2$ are the standard annihilation operators for the cavity ($\hat{\mathbf{a}}$) and the two qubits ($\hat{\mathbf{b}}_1$, and $\hat{\mathbf{b}}_2$), respectively. For numerical purposes, the Hilbert spaces for the qubit and cavity are truncated after 6, respectively 70, levels. It has been verified that the inclusion of additional levels yields no significant change in the results of the subsequent sections. The parameters take the values listed in Table 1. The system is driven by the microwave field $\epsilon(t)$, with a pulse duration T. An off-resonant pulse results in a state-dependent shift of the resonator frequency [32]. For a slowly-varying pulse shape with $\epsilon(0) = \epsilon(T) = 0$, such that the level shifts occur adiabatically, the dynamics result in a geometric phase on each of the qubit levels. That is, the resulting gate takes the diagonal form

$$\hat{\mathbf{U}} = \mathrm{diag}\left[e^{i\phi_{00}}, e^{i\phi_{01}}, e^{i\phi_{10}}, e^{i\phi_{11}} \right]. \qquad (2)$$
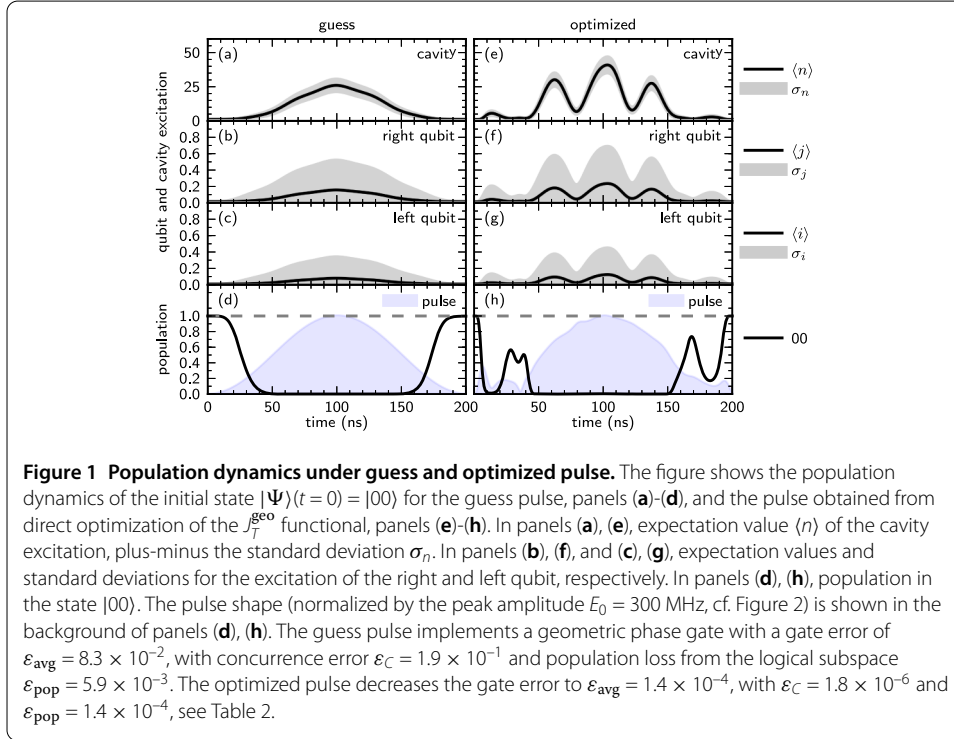
The maximal reachable concurrence of such a diagonal gate is

$$C(\gamma) = \left| \sin\left(\frac{\gamma}{2} \right) \right|, \quad \gamma \equiv \phi_{00} - \phi_{10} - \phi_{01} + \phi_{11}, \qquad (3)$$

where γ defines the non-local two-qubit phase [26]. The concurrence is obtained from the theory of local invariants for two-qubit gates [37, 38]. The local invariants for a diagonal gate evaluate to $G_1 = \cos^2(\gamma/2)$ and $G_2 = 1 + 2\cos^2(\gamma/2)$. From these, the Weyl chamber coordinates may be calculated as $c_1 = \gamma/2, c_2 = c_3 = 0$ [38]. Following Ref. [39], the concurrence is evaluated as a function of the Weyl chamber coordinates to yield Eq. (3). The gate is a perfect entangler for $\gamma = \pi$.

Table 1 Parameters for two transmon qubits coupled via a shared transmission line resonator

Cavity frequency	ω_c	8.10	GHz
Left qubit frequency	ω_1	6.85	GHz
Right qubit frequency	ω_2	7.25	GHz
Drive frequency	ω_d	8.14	GHz
Qubit anharmonicity	α_1, α_2	−300	MHz
Qubit-cavity coupling	g_1, g_2	70	MHz

Figure 1 Population dynamics under guess and optimized pulse. The figure shows the population dynamics of the initial state $|\Psi\rangle(t = 0) = |00\rangle$ for the guess pulse, panels (**a**)-(**d**), and the pulse obtained from direct optimization of the J_T^{geo} functional, panels (**e**)-(**h**). In panels (**a**), (**e**), expectation value $\langle n \rangle$ of the cavity excitation, plus-minus the standard deviation σ_n. In panels (**b**), (**f**), and (**c**), (**g**), expectation values and standard deviations for the excitation of the right and left qubit, respectively. In panels (**d**), (**h**), population in the state $|00\rangle$. The pulse shape (normalized by the peak amplitude $E_0 = 300$ MHz, cf. Figure 2) is shown in the background of panels (**d**), (**h**). The guess pulse implements a geometric phase gate with a gate error of $\varepsilon_{\text{avg}} = 8.3 \times 10^{-2}$, with concurrence error $\varepsilon_C = 1.9 \times 10^{-1}$ and population loss from the logical subspace $\varepsilon_{\text{pop}} = 5.9 \times 10^{-3}$. The optimized pulse decreases the gate error to $\varepsilon_{\text{avg}} = 1.4 \times 10^{-4}$, with $\varepsilon_C = 1.8 \times 10^{-6}$ and $\varepsilon_{\text{pop}} = 1.4 \times 10^{-4}$, see Table 2.

We consider pulse shapes of the form

$$\epsilon(t) = E_0 \sin^2\left(\pi \frac{t}{T}\right) \cos(\omega_d t) \tag{4}$$

with a fixed driving frequency ω_d given in Table 1. For simplicity, we neglect the dephasing induced by high cavity populations which allows solution of wave-packet dynamics with the time-dependent Schrödinger equation including microwave control fields. For an arbitrarily chosen guess pulse of duration $T = 200$ ns and peak amplitude $E_0 = 300$ MHz, the population dynamics resulting from the initial condition $|\Psi(t = 0)\rangle = |00\rangle$ are shown in panels (a)-(d) of Figure 1.

If the pulse induces adiabatic dynamics, it shifts the qubit and cavity levels proportionally to $\epsilon(t)^2/\Delta$ where Δ is the detuning from the respective level [32]. In the original field-free frame, this is equivalent to shifting the initial wave packet proportionally to the square of the pulse. Thus, the excitation and population dynamics should smoothly follow the pulse shape. Specifically, the condition for adiabaticity is that if the pulse shape were to be stretched in time, the population dynamics would simply stretch correspondingly. For a given peak amplitude, the larger the detuning of the drive ω_d from the frequencies $\omega_c, \omega_2, \omega_1$, the smaller the excitation in the respective Hilbert space. Since the

drive is detuned by only 40 MHz from the cavity, the cavity excitation, panel (a), reaches a large value $\langle n \rangle \approx 30$. The far-detuned right qubit, panel (b), and even farther detuned left qubit, panel (c), only show a small excitation. As indicated by the standard deviations shown as shaded areas in panels (a)-(c), the excitation remains relatively localized in energy. It is noteworthy, however, that the excitation curves (specifically of the cavity) show some imperfections. These 'wobbles' can be interpreted as deviations from the expected adiabatic dynamics, e.g. jumping over an avoided crossing between highly excited cavity states. This ultimately results in a small loss of population from the logical subspace, as the system does not perfectly return to its original state. The loss of population for the given example is $\varepsilon_{\text{pop}} = 5.9 \times 10^{-3}$. While such a small deviation is not discernible in the plot of the population in panel (d), it is nonetheless a significant error in the objective of obtaining high fidelity gates below the quantum error correction limit, typically resulting in gate errors below 10^{-3}. In principle, cavity population can be suppressed by tuning the qubit parameters and using non-trivial pulse shapes [32].

The dynamics for the remaining two-qubit basis states are similar to those of the $|00\rangle$ state in Figure 1. The concurrence of the gate implemented by the propagated guess pulse, according to Eq. (3), yields a value of $C \approx 0.8$. This implements the closest diagonal perfect entangler with an average gate error of 8.3×10^{-2}. Both the loss of population from the logical subspace and the small value of the generated entanglement imply that the chosen pulse parameters are sub-optimal with respect to the desired geometric phase gate. We therefore turn to numerical optimal control to obtain a high fidelity gate.

3 Direct optimization with Krotov's method

3.1 Optimization functionals and method

The standard approach for implementing a specific quantum gate $\hat{\mathbf{O}}$ using optimal control theory is to maximize the overlap between the time evolution $\hat{\mathbf{U}}(T, 0; \epsilon(t))$ under the control $\epsilon(t)$ and the target gate [19]. For a two-qubit gate, this is commonly expressed in the final time functional [40]

$$J_T^{\text{sm}} = 1 - \frac{1}{16}\left|\sum_{k=1}^{4} \langle k|\hat{\mathbf{O}}^\dagger \hat{\mathbf{U}}\big(T, 0; \epsilon(t)\big)|k\rangle\right|^2, \quad |k\rangle \in \big\{|00\rangle, |01\rangle, |10\rangle, |11\rangle\big\}, \tag{5}$$

which goes to zero as the target gate $\hat{\mathbf{O}}$ is implemented, up to a global phase.

Krotov's method allows to iteratively improve the control field, changing the control $\epsilon^{(i)}(t)$ to the updated control $\epsilon^{(i+1)}(t)$ in the ith iteration. The final time functional J_T, given e.g. by Eq. (5), is augmented with a running cost to result in the total functional

$$J\big[\epsilon^{(i)}(t)\big] = J_T\big(\{\phi_k^{(i)}(T)\}\big) + \int_0^T g_a\big[\epsilon^{(i)}(t)\big]\,dt, \qquad |\phi_k^{(i)}(t)\rangle = \hat{\mathbf{U}}\big(t, 0; \epsilon^{(i)}(t)\big)|k\rangle. \tag{6}$$

Monotonic convergence is ensured by the choice [9, 40]

$$g_a\big[\epsilon^{(i)}(t)\big] = \frac{\lambda_a}{S(t)}\big(\Delta\epsilon(t)\big)^2, \quad \Delta\epsilon(t) \equiv \epsilon^{(i+1)}(t) - \epsilon^{(i)}(t), \tag{7}$$

where λ_a is an arbitrary scaling parameter and $S(t) \in [0, 1]$ is a shape function that ensures smooth switch-on and switch-off.

The iterative update scheme is then given in terms of three coupled equations [9],

$$\Delta\epsilon(t) = \frac{S(t)}{\lambda_a} \text{Im}\left[\sum_{k=1}^{4}\left(\langle\chi_k^{(i)}(t)|\left(\frac{\partial\hat{\mathbf{H}}}{\partial\epsilon}\bigg|_{\substack{\phi^{(i+1)}(t)\\ \epsilon^{(i+1)}(t)}}\right)|\phi_k^{(i+1)}(t)\rangle\right.\right.$$

$$\left.\left. + \frac{1}{2}\sigma(t)\langle\Delta\phi_k(t)|\left(\frac{\partial\hat{\mathbf{H}}}{\partial\epsilon}\bigg|_{\substack{\phi^{(i+1)}(t)\\ \epsilon^{(i+1)}(t)}}\right)|\phi_k^{(i+1)(t)}\rangle\right)\right], \tag{8a}$$

$$\frac{\partial}{\partial t}|\phi_k^{(i+1)}(t)\rangle = -\frac{i}{\hbar}\hat{\mathbf{H}}^{(i+1)}|\phi_k^{(i+1)}(t)\rangle, \qquad |\phi_k^{(i+1)}(0)\rangle = |k\rangle, \tag{8b}$$

$$\frac{\partial}{\partial t}|\chi_k^{(i)}(t)\rangle = -\frac{i}{\hbar}\hat{\mathbf{H}}^{\dagger(i)}|\chi_k^{(i)}(t)\rangle, \qquad |\chi_k^{(i)}(T)\rangle = -\frac{\partial J_T}{\partial\langle\phi_k|}\bigg|_{\phi_k^{(i)}(T)}, \tag{8c}$$

with $|\Delta\phi_k(t)\rangle \equiv |\phi_k^{(i+1)}(t)\rangle - |\phi_k^{(i)}(t)\rangle$. The second order contribution to the update, with the prefactor $\sigma(t)$, is required for certain types of functionals [9], as we will see below. For the choice of J_T^{sm}, we may set $\sigma(t) = 0$ [9].

For the gate mechanism outlined in Section 2, we obtain a phase on each of the four logical basis states. These phases should combine to produce a perfect entangler, with $\gamma = \pi$ according to Eq. (3). The individual phases ϕ_{00}, ϕ_{01}, ϕ_{10} and ϕ_{11} depend delicately on the shape, amplitude, and duration of the pulse. It is therefore not known *a priori* for a given guess pulse which exact geometric phase gate will or can be reached, and thus what should be the target gate $\hat{\mathbf{O}}$ of the optimization. For a gate $\hat{\mathbf{U}}_0$ induced by a guess pulse, we may construct the *closest* diagonal perfect entangler by numerically evaluating

$$\hat{\mathbf{O}} = \underset{\phi_{00},\phi_{01},\phi_{10}}{\arg\min}\left\|\hat{\mathbf{O}}_{\text{diag}}(\phi_{00},\phi_{01},\phi_{10}) - \hat{\mathbf{U}}_0\right\|, \tag{9}$$

with

$$\hat{\mathbf{O}}_{\text{diag}}(\phi_{00},\phi_{01},\phi_{10}) = \text{diag}\left[e^{i\phi_{00}}, e^{i\phi_{01}}, e^{i\phi_{10}}, e^{i(\pi+\phi_{01}+\phi_{10}-\phi_{00})}\right], \tag{10}$$

which includes the condition $\gamma = \pi$ to make the gate a perfect entangler. Using this gate as a target fully determines the optimization problem, with two caveats. First, the target gate depends on $\hat{\mathbf{U}}_0$ induced by the (arbitrary) guess pulse, and second, the construction of the closest diagonal perfect entangler does not take into account the topology of the optimization landscape; the 'closest' gate is by no means guaranteed to be the one that is easiest to reach.

An approach that addresses these issues is to go beyond the standard functional of Eq. (5) and formulate a functional that targets the properties of the geometric phase gate specifically, without stipulating the phases on all of the logical states. We split the functional into two terms,

$$J_T^{\text{geo}} = \frac{1}{8}(J_{\text{diag}} + J_\gamma), \tag{11}$$

where J_{diag} goes to zero if and only if the gate is diagonal (with arbitrary phases) and J_γ goes to zero if and only if the gate is also a perfect entangler, $\gamma = \pi$. Thus, the functional

is conceptually similar to a recently proposed functional targeting an arbitrary perfect entangler [41]. However, the additional restriction to enforce a diagonal gate is important, as the Hamiltonian also allows for non-diagonal gates, but only through undesired non-adiabatic effects.

The two terms take the form

$$J_{\text{diag}} = 4 - \tau_{00}\tau_{00}^* - \tau_{01}\tau_{01}^* - \tau_{10}\tau_{10}^* - \tau_{11}\tau_{11}^*, \tag{12a}$$

$$J_\gamma = 2 + \tau_{00}\tau_{01}^*\tau_{10}^*\tau_{11} + \tau_{00}^*\tau_{01}\tau_{10}\tau_{11}^*, \tag{12b}$$

with

$$\begin{aligned}
\tau_{00} &\equiv \langle 00|\hat{\mathbf{U}}|00\rangle, & \tau_{01} &\equiv \langle 01|\hat{\mathbf{U}}|01\rangle, \\
\tau_{10} &\equiv \langle 10|\hat{\mathbf{U}}|10\rangle, & \tau_{11} &\equiv \langle 11|\hat{\mathbf{U}}|11\rangle.
\end{aligned} \tag{12c}$$

The construction of J_γ is based on the observation that

$$\gamma = \pi \quad \Longleftrightarrow \quad 2 + e^{i\gamma} + e^{-i\gamma} = 0,$$

which becomes Eq. (12b) by associating τ_k with $e^{i\phi_k}$ and using the definition of γ in Eq. (3). Both J_{diag} and J_γ take values $\in [0, 4]$, hence the normalization factor $\frac{1}{8}$ in Eq. (11) to bring the value of the functional closer to that of J_T^{sm}.

In contrast to J_T^{sm}, the functional J_T^{geo} is *not* convex, since the states enter in higher than quadratic order. The Krotov update equation (8a) must then include the second order contribution, where $\sigma(t)$ can be determined numerically in each iteration as [9]

$$\sigma(t) = -\max(\epsilon_A, 2A + \epsilon_A), \quad A = \frac{2\sum_{k=1}^4 \text{Re}[\langle \chi_k(T)|\Delta\phi_k(T)\rangle] + \Delta J_T}{\sum_{k=1}^4 |\Delta\phi_k(T)|^2}, \tag{13}$$

with a small non-negative number ϵ_A, and $\Delta J_T \equiv J_T(\{\phi_k^{(i+1)}(T)\}) - J_T(\{\phi_k^{(i)}(T)\})$. The boundary condition for the backward propagated states in Eq. (8c) yields

$$\big|\chi_{00}(T)\big\rangle = \big(\tau_{00} - \tau_{01}\tau_{10}\tau_{11}^*\big)|00\rangle, \tag{14a}$$

$$\big|\chi_{01}(T)\big\rangle = \big(\tau_{01} - \tau_{00}\tau_{10}^*\tau_{11}\big)|01\rangle, \tag{14b}$$

$$\big|\chi_{10}(T)\big\rangle = \big(\tau_{10} - \tau_{00}\tau_{01}^*\tau_{11}\big)|10\rangle, \tag{14c}$$

$$\big|\chi_{11}(T)\big\rangle = \big(\tau_{11} - \tau_{00}^*\tau_{01}\tau_{10}\big)|11\rangle. \tag{14d}$$

Both J_T^{sm} and J_T^{geo} are only loosely connected to the *average gate fidelity* that is accessible to experimental measurement. In the case of a two-qubit gate and non-dissipative dynamics this can be evaluated as [42]
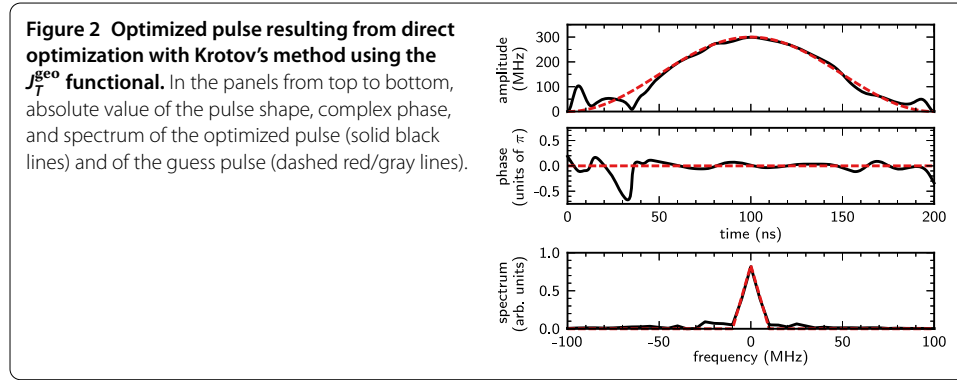
$$F_{\text{avg}} = \int \big|\langle \Psi|\hat{\mathbf{O}}^\dagger\hat{\mathbf{U}}|\Psi\rangle\big|^2 \, d\Psi = \frac{1}{20}\big(\big|\text{tr}\big[\hat{\mathbf{O}}^\dagger\hat{\mathbf{U}}\big]\big|^2 + \text{tr}\big[\hat{\mathbf{O}}^\dagger\hat{\mathbf{U}}\hat{\mathbf{U}}^\dagger\hat{\mathbf{O}}\big]\big). \tag{15}$$

Thus, F_{avg}, respectively the gate error $\varepsilon_{\text{avg}} \equiv 1 - F_{\text{avg}}$, provides a well-defined measure of the optimization success independent of the choice of optimization functional. For an optimization with J_T^{geo}, we may evaluate ε_{avg} with respect to the closest geometric phase gate resulting from propagation with the optimized pulse, according to Eq. (9).

Table 2 Optimization success for different optimization schemes

	T [ns]	prop.	ε_C	ε_{pop}	ε_{avg}
Guess	200	0	1.92×10^{-1}	5.94×10^{-3}	8.25×10^{-2}
Direct s.m.	200	20,000	2.23×10^{-2}	4.13×10^{-3}	1.45×10^{-2}
Direct geo.	200	11,032	1.83×10^{-6}	1.42×10^{-4}	1.43×10^{-4}
Simplex	185	116	1.95×10^{-5}	1.40×10^{-2}	1.40×10^{-2}
Pre-opt. s.m.	185	518	5.07×10^{-5}	1.11×10^{-5}	3.36×10^{-5}
Pre-opt. geo.	185	300	5.24×10^{-5}	1.40×10^{-5}	3.50×10^{-5}

For each scheme, we give the gate duration T, the total number of propagations, the concurrence error $\varepsilon_C \equiv 1 - C$ by which the gate differs from a perfect entangler, the loss of population ε_{pop} from the logical subspace, and the gate error $\varepsilon_{\text{avg}} \equiv 1 - F_{\text{avg}}$ with respect to a geometric phase gate. The number of propagations for 'pre-opt. s.m.' and 'pre-opt. geo.' include both the 116 propagations of the first stage simplex optimization and the propagations from the second-stage optimization using Krotov's method, with 201 respectively 92 iterations, and two propagations per iteration. The reported number of propagations is thus proportional to the total CPU and wall-clock time required to obtain the result starting from the original guess pulse.

Figure 2 Optimized pulse resulting from direct optimization with Krotov's method using the J_T^{geo} functional. In the panels from top to bottom, absolute value of the pulse shape, complex phase, and spectrum of the optimized pulse (solid black lines) and of the guess pulse (dashed red/gray lines).

3.2 Optimization results

The optimization starts from the guess pulse described by Eq. (4), with $T = 200$ ns and $E_0 = 300$ MHz, as discussed in Section 2, with the dynamics shown in panels (a)-(d) of Figure 1. The gate error with respect to the closest geometric phase gate for this guess is $\varepsilon_{\text{avg}} = 8.3 \times 10^{-2}$, with a loss of population from the logical subspace of $\varepsilon_{\text{pop}} = 5.9 \times 10^{-3}$. The concurrence error, defined as $\varepsilon_C \equiv 1 - C$, takes the value 1.9×10^{-1}.

Optimization using Krotov's method and J_T^{geo} as the optimization functional converges within 5,516 iterations of the algorithm. Convergence is assumed when the relative change of the functional $\Delta J_T / J_T$ falls below 10^{-4}, such that no significant further improvement is to be expected. The gate error is reduced to $\varepsilon_{\text{avg}} = 1.4 \times 10^{-4}$. It is dominated by the remaining loss of population from the logical subspace, $\varepsilon_{\text{pop}} \approx \varepsilon_{\text{avg}}$, as the concurrence error is only $\varepsilon_C = 1.8 \times 10^{-6}$, see Table 2.

The resulting optimized pulse is shown in Figure 2, with the guess pulse indicated by the dashed line. For the center 100 ns, there are only small deviations from the guess pulse (both in shape and phase). Significant deviations occur only at the very beginning and end, most notably the variation in the complex phase (center panel) between 20 and 40 ns. The spectral width of the pulse (bottom panel) remains well within a bandwidth of ± 50 MHz. The dynamics of the $|00\rangle$ state under the optimized pulse are shown in panels (e)-(h) of Figure 1. The difference to the dynamics under the guess pulse, panels (a)-(d), is striking; the excitations no longer smoothly follow the pulse shape, but show strong oscillations on top of the expected behavior. The features at the beginning of the optimized pulse provide a kick to the system, inducing oscillations in the populations, with a counter-kick near the

end of the pulse. These kicks are very visible in the population of the $|00\rangle$ state in panel (h), compared to the smooth dynamics for guess pulse in panel (d).

It is worth noting that the gate obtained with the optimized pulse is *not* the closest geometric phase gate to the gate implemented by the guess pulse, as in Eq. (9). This illustrates the benefit of using J_T^{geo} over J_T^{sm}. The latter optimizes towards a specific, pre-determined gate, according to Eq. (9), while J_T^{geo} can dynamically adjust which specific geometric phase gate is easiest to reach, allowing it to fulfill the objective much more easily. Table 2 shows that optimization with J_T^{geo} requires significantly less propagations (which are directly proportional to CPU time) than optimization with J_T^{sm}, for both direct and pre-optimized strategies.

While the optimization yields a gate error well below the quantum error correction threshold, it deviates significantly from the simple geometric phase gate scheme, resulting in complex dynamics. The numerical effort required to obtain a high fidelity solution is considerable, with several thousand iterations (each iteration requiring two full propagations of four logical basis states). We have discussed here only the optimization for a fixed gate duration of $T = 200$ ns. Generally, significantly faster quantum gates could potentially be implemented using other mechanisms, e.g. [24]. The geometric phase gate, however, relies on adiabatic shifts of the energy levels such that loss of population from the logical subspace inhibits realization of high fidelities when pushing the gate duration significantly below 200 ns.

The complexity of the optimized pulse is typical for Krotov's method or other gradient-based optimization methods. For the present example, this clashes with the gate mechanism of the geometric phase gate that intends to use simple and smooth pulse shapes.
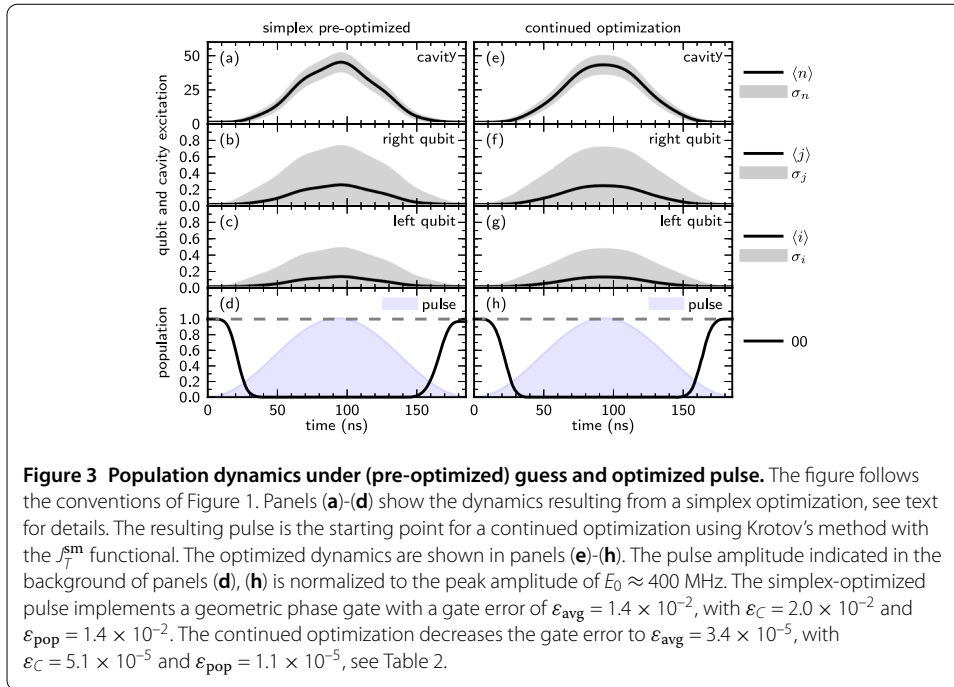
4 Hybrid optimization scheme

4.1 Simplex optimization

The gate error of the guess pulse is dominated by the insufficient amount of entanglement that is generated. A natural approach is to maintain the analytical pulse shape of Eq. (4) for the time being, and to vary the free parameters E_0 and T in order to maximize the figure of merit. Such an optimization of a pulse determined by only a handful of parameters (in this case two) is easily performed using a gradient-free method such as Nelder-Mead simplex. This has the additional benefit that there are no restrictions on the choice of optimization functional. Specifically, there is no need to formulate it in such a way that derivatives can be calculated analytically. Thus, we can include the objective of minimizing the gate duration in the functional and modify Eq. (11) to read

$$J_T^{\text{splx}} = J_{\text{diag}} + J_\gamma + \frac{T}{T_0}, \quad T_0 = 200 \text{ ns}. \tag{16}$$

Note that with the addition of penalizing the gate duration, the functional is no longer a distance measure that approaches zero as the target is reached; the simplex optimization will find a local minimum of Eq. (16) at a value of $J_T^{\text{splx}} \lesssim 1$.

Using only 116 propagations, the algorithm converges to a solution that reduces the gate duration from 200 to 185 ns, while bringing the entanglement error down to $\varepsilon_C = 2.0 \times 10^{-5}$, see Table 2. The resulting dynamics are shown in panels (a)-(d) of Figure 3. They are similar to those of the original guess pulse, cf. panel (a)-(d) of Figure 1. The shorter pulse duration and larger pulse intensity (from 300 MHz in the original guess to $\approx$400 MHz)
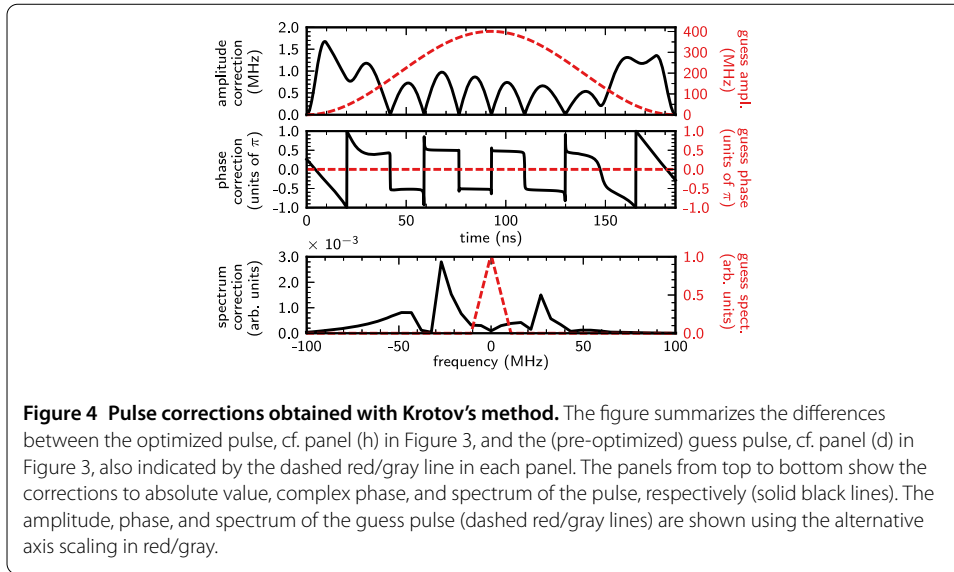
Figure 3 Population dynamics under (pre-optimized) guess and optimized pulse. The figure follows the conventions of Figure 1. Panels (**a**)-(**d**) show the dynamics resulting from a simplex optimization, see text for details. The resulting pulse is the starting point for a continued optimization using Krotov's method with the J_T^{sm} functional. The optimized dynamics are shown in panels (**e**)-(**h**). The pulse amplitude indicated in the background of panels (**d**), (**h**) is normalized to the peak amplitude of $E_0 \approx 400$ MHz. The simplex-optimized pulse implements a geometric phase gate with a gate error of $\varepsilon_{\mathrm{avg}} = 1.4 \times 10^{-2}$, with $\varepsilon_C = 2.0 \times 10^{-2}$ and $\varepsilon_{\mathrm{pop}} = 1.4 \times 10^{-2}$. The continued optimization decreases the gate error to $\varepsilon_{\mathrm{avg}} = 3.4 \times 10^{-5}$, with $\varepsilon_C = 5.1 \times 10^{-5}$ and $\varepsilon_{\mathrm{pop}} = 1.1 \times 10^{-5}$, see Table 2.

results in a significantly larger cavity excitation. It also leads to more non-adiabatic defects (wobbles in the cavity excitation). Consequently, the loss of population from the logical subspace is increased by about a factor of two to $\varepsilon_{\mathrm{pop}} = 1.4 \times 10^{-2}$, and limits the total gate error to $\varepsilon_{\mathrm{avg}} = 1.4 \times 10^{-2}$. Thus, while the simplex search yields a dramatic improvement over the original guess pulse, it does not reach a sufficiently high fidelity to approach the quantum error correction limit. To remedy this, we turn to a hybrid approach, combining simplex and gradient-based optimization.

4.2 Continued optimization with Krotov's method

For the present example, we use the final pulse of the previous section as the starting point of an optimization with Krotov's method. Since now the guess pulse already has a relatively high fidelity, both the J_T^{sm} and J_T^{geo} functionals may be used interchangeably, as we are only searching in a very small vicinity of the starting point. Both methods converge rapidly to $\Delta J_T / J_T < 10^{-4}$ in under 200 iterations. The dynamics resulting from the propagation of the $|00\rangle$ state under the pulse obtained from optimization with the J_T^{sm} functional is shown in panels (e)-(h) of Figure 3. The comparison to the dynamics of the pre-optimized guess pulse in panels (a)-(d) is striking: the excitations now follow the pulse shape smoothly. The non-adiabatic defects, i.e., the wobbles especially in the cavity excitation in panel (a), have been corrected. Consequently, the loss of population from the logical subspace is now reduced to a value of $\varepsilon_{\mathrm{pop}} = 1.1 \times 10^{-5}$. Together with only a slight increase in the concurrence error to $\varepsilon_C = 5.1 \times 10^{-5}$, the overall gate error of the optimized pulse is $\varepsilon_{\mathrm{avg}} = 3.4 \times 10^{-5}$. This is an improvement of half an order of magnitude compared to the direct optimization in Section 3.2. Moreover, the result has been obtained at a small fraction of the numerical cost. The pre-optimized guess and post-optimized pulse shape, indicated as the blue shaded area in panels (d) and (h), appear visually indistinguishable.
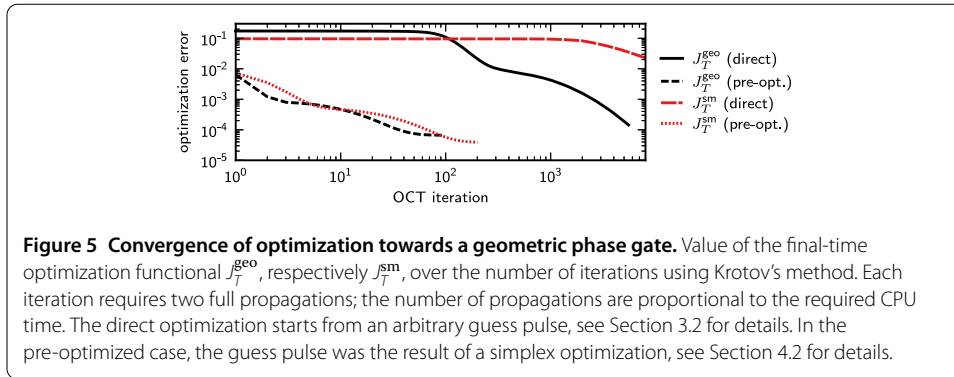
The correction to the pre-optimized guess pulse is shown in Figure 4. Indeed, the corrections are on the order of 1 MHz, much smaller than the peak amplitude of $E_0 \approx 400$ MHz.

Figure 4 Pulse corrections obtained with Krotov's method. The figure summarizes the differences between the optimized pulse, cf. panel (h) in Figure 3, and the (pre-optimized) guess pulse, cf. panel (d) in Figure 3, also indicated by the dashed red/gray line in each panel. The panels from top to bottom show the corrections to absolute value, complex phase, and spectrum of the pulse, respectively (solid black lines). The amplitude, phase, and spectrum of the guess pulse (dashed red/gray lines) are shown using the alternative axis scaling in red/gray.

The corrections follow a regular pattern, both in the shape (top panel) and the complex phase (center panel), as indicated by the existence of sharp peaks in the spectrum (bottom panel). It appears that the non-adiabatic defects in the pre-optimized guess pulse can be corrected by a series of small kicks in amplitude and phase at regular intervals. This results in an optimized pulse that is conceptually simpler and yields a higher fidelity than the direct application of Krotov's method. The comparison illustrates the power of a hybrid approach to steer the *physical* characteristics of the optimized control. In our example, the parametrization used in the first optimization stage enforces the desired pulse shape. Without this restriction, pulses of undesirable complexity are obtained. On the other hand, the restriction must ultimately be relaxed to allow for the representation of the higher-frequency features that correct non-adiabatic defects. Thus, the role of the two-stage optimization is also to influence the physical features of the control, in addition to its numerical benefits.

The striking numerical efficiency of the hybrid optimization scheme can be seen by comparing its convergence to that of the direct optimization. This is shown in Figure 5. The direct optimization shows an extended plateau for at least the first 100 iterations, before slowly converging. This behavior is typical for ill-chosen guess pulses [43]. For a direct optimization with the J_T^{sm} functional, the plateau extends for several thousand iterations, and does not yield convergence within 10,000 iterations. In contrast, the optimization starting from a pre-optimized pulse has no plateau (note the log-scale of the x-axis); both J_T^{sm} and J_T^{geo} converge at roughly the same rate. The improvement by the simplex (pre-)optimization compared to the original guess pulse can be seen from the difference in the y-intercept between the 'direct' and 'pre-optimized' curves in Figure 5; in addition, there is also a reduction in the gate duration from 200 to 185 ns at no additional numerical cost.

The gate duration for the geometric phase gate mechanism is limited by the requirement of adiabaticity. We have also performed the hybrid optimization scheme for a gate duration of ≈100 ns. In this case, the simplex search yields significant non-adiabatic defects, with a loss of population of 1.2×10^{-1}. The concurrence error is 2.3×10^{-3} and the total gate error, $\varepsilon_{\mathrm{avg}} = 1.2 \times 10^{-1}$, is dominated by the population loss. Post-optimization using Krotov's

Figure 5 Convergence of optimization towards a geometric phase gate. Value of the final-time optimization functional J_T^{geo}, respectively J_T^{sm}, over the number of iterations using Krotov's method. Each iteration requires two full propagations; the number of propagations are proportional to the required CPU time. The direct optimization starts from an arbitrary guess pulse, see Section 3.2 for details. In the pre-optimized case, the guess pulse was the result of a simplex optimization, see Section 4.2 for details.

method significantly reduces the total gate error to $\varepsilon_{\text{avg}} = 1.4 \times 10^{-2}$. The post-optimization result is obtained at a numerical cost very close to that for the $T = 200$ ns gate, and yields pulse corrections very similar to those shown in Figure 4. This results in a correction of the non-adiabatic defects and thereby lowers the population loss to only 6.5×10^{-3}. The total gate error is now dominated instead by the increased concurrence error of 1.7×10^{-2}, which is insufficient for a high quality phase gate. The observation that an overall improvement in gate performance at $T = 100$ ns from hybrid optimization is only possible by increasing adiabaticity at the cost of reduced entanglement, indicates that a quantum speed limit has been reached for the specific gate mechanism. These results show that a hybrid optimization scheme may be used successfully even when operating close to the quantum speed limit.

While it is not the aim of this work to characterize the quantum speed limit for the coupled transmon system, we note that this could be quantified by systematically scanning over the gate duration [26]. Under the constraints of the specific gate mechanism employed here, a numerical approach appears necessary to extract the speed limit. However, for the Strauch gate of Ref. [44], an analytic estimate may be made from summing the minimal precession periods required for each component of the gate, i.e., two iSWAP and one controlled-Z gates. With the qubit-cavity interaction strength of $g = 70$ MHz employed here, this would suggest that gate durations as short as a few tens of nanoseconds might be attainable for this system.

We may also compare the total number of propagations necessary to obtain the optimized pulse, included in Table 2 together with measures of success: concurrence error, loss of population from the logical subspace, and gate error. Each iteration using Krotov's method requires two propagations. For the hybrid optimization schemes ('pre-opt s.m.', 'pre-opt hol.'), the number of propagations includes simplex as well as the additional propagations due to Krotov's method. The gate error is measured with respect to the exact target gate when using the square-modulus functional, and with respect to the closest geometric phase gate to the optimized dynamics in all other cases. In terms of numerical efficiency, the hybrid schemes outperform the direct optimization by nearly two orders of magnitude while resulting in a significantly better gate fidelity.

5 Conclusions

For the example of a geometric phase gate on a system of two transmon qubits with a shared transmission line resonator, we have considered the application of gradient-based optimization methods, specifically Krotov's method, and a gradient-free optimization

method, Nelder-Mead simplex. The objectives of the geometric phase gate can be formulated in a specialized optimization functional J_T^{geo} that reaches its optimal value for any diagonal perfect entangler. We have shown that for a direct optimization, this functional vastly outperforms the 'standard' square-modulus functional for gate optimization. Convergence is aided by the use of a functional that formulates the objective as general as possible. This is in agreement with recent results for optimization using a functional targeting arbitrary perfect entanglers [41, 45].

The direct optimization using Krotov's method can in principle find controls that implement the desired gate with high fidelity. However, the resulting dynamics are complex and the numerical effort is dominated by an extended plateau in the initial phase of the optimization; for short gate durations, optimization becomes increasingly harder and the fidelity is limited by loss from the logical subspace. The numerical effort to reach high fidelities quickly becomes unfeasible in this case. In contrast, parametrizing the pulse by its duration and peak amplitude only, and applying a simplex optimization on those parameters, we are able to find a simple analytic pulse that implements the desired gate with moderate fidelity, still one order of magnitude above the quantum error correction limit. Thus, for the example presented here, neither the application of a gradient-based algorithm nor the simplex optimization alone yield satisfactory results; only the combination of both methods into a hybrid optimization scheme is able to obtain controls with a clear mechanism that implement a geometric phase gate to high fidelity, with a minimum of numerical effort.

These results prompt the recommendation to generally adapt hybrid optimization schemes, i.e., obtain guess pulses for gradient-based optimization from a gradient-free pre-optimization, when there is insufficient knowledge to design good guess pulses by hand. There is great flexibility in the choice of parametrization. Here, we have taken the two free parameters, peak amplitude and gate duration, in a simple fixed analytical formula for the pulse shape. Generally, one might use slightly more sophisticated parametrizations, following e.g. the CRAB approach [18]. The small number of free parameters and relatively high quality of the original guess pulse with a fidelity of already >90% results in particularly fast convergence of the simplex method. For a more sophisticated example, at least several hundred propagations would probably be required in the simplex stage. However, even in that case, this numerical effort is by far outweighed by the large number of iterations required to leave the initial plateau in the optimization landscape for a bad guess pulse in a direct gradient-based optimization. Moreover, any figure of merit is suitable for optimization with the simplex method, as there is no need to derive the gradient for the optimization functional. For example, the gate duration can be included in the figure of merit, something that generally is not straightforward in gradient-based methods [46]. The hybrid scheme is aimed at providing optimal solutions in an open-loop context, and still leaves open the possibility of further combining open-loop and closed-loop optimization methods when targeting a specific experimental setup [47].

In principle, the approach could thus be extended to multiple stages, where in each stage, a different parameterization and a suitable optimization algorithm is used. There is no requirement for a specific method such as Nelder-Mead simplex or Krotov's method to be employed. For example, a two-stage optimization using a genetic algorithm in the first stage, and a gradient algorithm in the second stage has been used for the optimization of quantum gates in strongly coupled two-level systems [48, 49]. There, starting with a simple

parametrization, and then moving to a less restricted search space in the second optimization stage was also found to benefit the overall optimization performance, in agreement with the results shown here.

Adding an additional stage might also be beneficial when the optimization landscape is non-trivial and contains traps or saddle points. This may happen e.g. when the optimization is performed with limited resources [50]. Repeating the simplex search from a different starting point - either by systematic variation or by random search - may then find solutions that do not get stuck in traps of the optimization landscape. Of course, the truncation of the search space due to the low-dimensional parametrization may itself introduce additional traps in the landscape. However, these traps would disappear when returning to the full search space in the final optimization stage.

For the specific example of the geometric phase gate considered here, we have found the post-optimization to introduce small corrections to non-adiabatic defects. Due to the small relative strength of the correction, the experimental realization of the geometric phase gate would require extraordinary precision. Moreover, the large excitation of the cavity would limit the fidelity when dissipative effects, specifically spontaneous decay of the cavity are taken into account. However, we stress that the method of employing hybrid optimization schemes presented here is entirely general and aimed at reducing the numerical effort in obtaining high fidelity solutions to arbitrary quantum control problems, not limited to quantum information processing. Moreover, robustness with respect to both fluctuations in the control parameters and dissipation can be achieved using complimentary advanced control techniques, such as a description in Liouville space and ensemble optimization [31, 43]. These approaches are numerically even more demanding, such that the reduction of the optimization cost achieved by the hybrid scheme discussed here may become imperative.

Author details
[1]Theoretische Physik, Universität Kassel, Heinrich-Plett-Str. 40, Kassel, D-34132, Germany. [2]Department of Chemistry, University of California, Berkeley, CA 94720, USA.

References
 1. Brumer P, Shapiro M. Principles and applications of the quantum control of molecular processes. New York: Wiley; 2003.
 2. Rice SA, Zhao M. Optical control of molecular dynamics. New York: Wiley; 2000.
 3. Tannor DJ, Rice SA. Control of selectivity of chemical reaction via control of wave packet evolution. J Chem Phys. 1985;83:5013.
 4. Tannor DJ, Kosloff R, Rice SA. Coherent pulse sequence induced control of selectivity of reactions: exact quantum mechanical calculations. J Chem Phys. 1986;85:5805.
 5. Levin L, Skomorowski W, Rybak L, Kosloff R, Koch CP, Amitay Z. Coherent control of bond making. Phys Rev Lett. 2015;114:233003.
 6. Brif C, Chakrabarti R, Rabitz H. Control of quantum phenomena: past, present and future. New J Phys. 2010;12:075008.
 7. Konnov AI, Krotov VF. On global methods of successive improvement of controlled processes. Autom Remote Control. 1999;60:1427.

8. Sklarz SE, Tannor DJ. Loading a Bose-Einstein condensate onto an optical lattice: an application of optimal control theory to the nonlinear Schrödinger equation. Phys Rev A. 2002;66(5):053619.
9. Reich DM, Ndong M, Koch CP. Monotonically convergent optimization in quantum control using Krotov's method. J Chem Phys. 2012;136:104103.
10. Khaneja N, Reiss T, Kehlet C, Schulte-Herbrüggen T, Glaser SJ. Optimal control of coupled spin dynamics: design of NMR pulse sequences by gradient ascent algorithms. J Magn Res. 2005;172:296.
11. Byrd RH, Lu P, Nocedal J, Zhu C. A limited memory algorithm for bound constrained optimization. SIAM J Sci Comput. 1995;16(5):1190.
12. de Fouquières P, Schirmer SG, Glaser SJ, Kuprov I. Second order gradient ascent pulse engineering. J Magn Res. 2011;212:412.
13. Eitan R, Mundt M, Tannor DJ. Optimal control with accelerated convergence: combining the Krotov and quasi-Newton methods. Phys Rev A. 2011;83(5):053426.
14. Machnes S, Sander U, Glaser S, de Fouquières P, Gruslys A, Schirmer S, Schulte-Herbrüggen T. Comparing, optimizing, and benchmarking quantum-control algorithms in a unifying programming framework. Phys Rev A. 2011;84:022305.
15. Judson RS, Rabitz H. Teaching lasers to control molecules. Phys Rev Lett. 1992;68:1500.
16. Goldberg DE. Genetic algorithms in search, optimization and machine learning. Boston: Addison-Wesley; 1989.
17. Doria P, Calarco T, Montangero S. Optimal control technique for many-body quantum dynamics. Phys Rev Lett. 2011;106:190501.
18. Caneva T, Calarco T, Montangero S. Chopped random-basis quantum optimization. Phys Rev A. 2011;84:022326.
19. Palao JP, Kosloff R. Quantum computing by an optimal control algorithm for unitary transformations. Phys Rev Lett. 2002;89:188301.
20. Tesch CM, de Vivie-Riedle R. Quantum computation with vibrationally excited molecules. Phys Rev Lett. 2002;89:157901.
21. Treutlein P, Hänsch TW, Reichel J, Negretti A, Cirone MA, Calarco T. Microwave potentials and optimal control for robust quantum gates on an atom chip. Phys Rev A. 2006;74:022312.
22. Schirmer S. Implementation of quantum gates via optimal control. J Mod Opt. 2009;56:831.
23. Müller MM, Reich DM, Murphy M, Yuan H, Vala J, Whaley KB, Calarco T, Koch CP. Optimizing entangling quantum gates for physical systems. Phys Rev A. 2011;84:042315.
24. Egger DJ, Wilhelm FK. Optimized controlled-z gates for two superconducting qubits coupled through a resonator. Supercond Sci Technol. 2014;27:014001.
25. Caneva T, Murphy M, Calarco T, Fazio R, Montangero S, Giovannetti V, Santoro GE. Optimal control at the quantum speed limit. Phys Rev Lett. 2009;103:240501.
26. Goerz MH, Calarco T, Koch CP. The quantum speed limit of optimal controlled phasegates for trapped neutral atoms. J Phys B. 2011;44:154011.
27. Bhattacharyya K. Quantum decay and the Mandelstam-Tamm-energy inequality. J Phys A. 1983;16:2993.
28. Margolus N, Levitin LB. The maximum speed of dynamical evolution. Physica D. 1998;120:188.
29. Kallush S, Kosloff R. Quantum governor: automatic quantum control and reduction of the influence of noise without measuring. Phys Rev A. 2006;73:032324.
30. Schulte-Herbrüggen T, Spörl A, Khaneja N, Glaser SJ. Optimal control for generating quantum gates in open dissipative systems. J Phys B. 2011;44:154013.
31. Goerz MH, Halperin EJ, Aytac JM, Koch CP, Whaley KB. Robustness of high-fidelity Rydberg gates with single-site addressability. Phys Rev A. 2014;90:032329.
32. Cross AW, Gambetta JM. Optimized pulse shapes for a resonator-induced phase gate. Phys Rev A. 2015;91:032325.
33. Rigetti C, Gambetta JM, Poletto S, Plourde BLT, Chow JM, Córcoles AD, Smolin JA, Merkel ST, Rozen JR, Keefe GA, Rothwell MB, Ketchen MB, Steffen M. Superconducting qubit in a waveguide cavity with a coherence time approaching 0.1 ms. Phys Rev B. 2012;86:100506.
34. Chow JM, Gambetta JM, Cross AW, Merkel ST, Rigetti C, Steffen M. Microwave-activated conditional-phase gate for superconducting qubits. New J Phys. 2013;15:115012.
35. Koch J, Yu TM, Gambetta J, Houck AA, Schuster DI, Majer J, Blais A, Devoret MH, Girvin SM, Schoelkopf RJ. Charge-insensitive qubit design derived from the Cooper pair box. Phys Rev A. 2007;76:042319.
36. Majer J, Chow JM, Gambetta JM, Koch J, Johnson BR, Schreier JA, Frunzio L, Schuster DI, Houck AA, Wallraff A, Blais A, Devoret MH, Girvin SM, Schoelkopf RJ. Coupling superconducting qubits via a cavity bus. Nature. 2007;449:443.
37. Makhlin Y. Nonlocal properties of two-qubit gates and mixed states, and the optimization of quantum computations. Quantum Inf Process. 2002;1(4):243.
38. Zhang J, Vala J, Sastry S, Whaley KB. Geometric theory of nonlocal two-qubit operations. Phys Rev A. 2003;67(4):042313.
39. Kraus B, Cirac JI. Optimal creation of entanglement using a two-qubit gate. Phys Rev A. 2001;63(6):062309.
40. Palao JP, Kosloff R. Optimal control theory for unitary transformations. Phys Rev A. 2003;68:062308.
41. Watts P, Vala J, Müller MM, Calarco T, Whaley KB, Reich DM, Goerz MH, Koch CP. Optimizing for an arbitrary perfect entangler: I. Functionals. Phys Rev A. 2015;91:062306.
42. Pedersen LH, Møller NM, Mølmer K. Fidelity of quantum operations. Phys Lett A. 2007;367:47.
43. Goerz MH, Reich DM, Koch CP. Optimal control theory for a unitary operation under dissipative evolution. New J Phys. 2014;16:055012.
44. Strauch FW, Johnson PR, Dragt AJ, Lobb CJ, Anderson JR, Wellstood FC. Quantum logic gates for coupled superconducting phase qubits. Phys Rev Lett. 2003;91:167005.
45. Goerz MH, Gualdi G, Reich DM, Koch CP, Motzoi F, Whaley KB, Vala J, Müller MM, Montangero S, Calarco T. Optimizing for an arbitrary perfect entangler. II. Application. Phys Rev A. 2015;91:062307.
46. Ndong M, Koch CP, Sugny D. Time optimization and state-dependent constraints in the quantum optimal control of molecular orientation. J Mod Opt. 2014;61(10):857.
47. Egger DJ, Wilhelm FK. Adaptive hybrid optimal quantum control for imprecisely characterized systems. Phys Rev Lett. 2014;112:240503.
48. Grace M, Brif C, Rabitz H, Walmsley IA, Kosut RL, Lidar DA. Optimal control of quantum gates and suppression of decoherence in a system of interacting two-level particles. J Phys B. 2007;40(9):103.

49. Grace MD, Brif C, Rabitz H, Lidar DA, Walmsley IA, Kosut RL. Fidelity of optimally controlled quantum gates with randomly coupled multiparticle environments. J Mod Opt. 2007;54:2339.
50. Moore KW, Rabitz H. Exploring constrained quantum control landscapes. J Chem Phys. 2012;137:134113.